

2011

Electrochemical glutamate biosensing with nanocube and nanosphere augmented single-walled carbon nanotube networks: A comparative study

Jonathan C. Claussen, *Purdue University*

Mayra S. Artiles, *Purdue University*

Eric S. McLamore, *Purdue University*

Subhashree Mohanty, *Purdue University*

Jin Shi, *Purdue University*, et al.

Electrochemical glutamate biosensing with nanocube and nanosphere augmented single-walled carbon nanotube networks: a comparative studyJonathan C. Claussen,^{ab} Mayra S. Artiles,^{ac} Eric S. McLamore,^{ab} Subhashree Mohanty,^{ad} Jin Shi,^{ad} Jenna L. Rickus,^{abd} Timothy S. Fisher^{ac} and D. Marshall Porterfield^{*abd}

Received 12th April 2011, Accepted 6th June 2011

DOI: 10.1039/c1jm11561h

We describe two hybrid nanomaterial biosensor platforms, based on networks of single-walled carbon nanotubes (SWCNTs) enhanced with Pd nanocubes and Pt nanospheres and grown *in situ* from a porous anodic alumina (PAA) template. These nanocube and nanosphere SWCNT networks are converted into glutamate biosensors by immobilizing the enzyme glutamate oxidase (cross-linked with glutaraldehyde) onto the electrode surface. The Pt nanosphere/SWCNT biosensor outperformed the Pd nanocube/SWCNT biosensor and previously reported similar nanomaterial-based biosensors by amperometrically monitoring glutamate concentrations with a wide linear sensing range (50 nM to 1.6 mM) and a small detection limit (4.6 nM, 3 σ). These results combined with the biosensor fabrication scheme (*in situ* growth of SWCNTs, electrodeposition of metal nanoparticles, and facile enzyme immobilization protocol) create a biosensor that can potentially be scaled for integration into a wide range of applications including the treatment of neurological disorders.

Introduction

The desire to detect and sense important physiological analytes with high sensitivity has fueled the recent marriage between nanotechnology and electrochemical biosensors. Indeed, advanced nanomaterials such as silicon nanowires, carbon nanotubes (CNTs), and metallic nanocrystals have significantly enhanced the electrical transduction of biomarkers associated with cancer, diabetes, and other genetic and infectious diseases.^{1–8} Electrochemical biosensor kinetics including heterogeneous charge transport at the electrode/liquid interface are substantially influenced by the biosensor surface characteristics including material, shape, and geometry.^{9–12} To this end, we herein present two distinct nanostructured biosensors that utilize networks of Pd nanocubes and Pt nanospheres electrically connected through single-walled carbon nanotubes (SWCNTs) to amperometrically sense varying concentrations of glutamate—a primary excitatory neurotransmitter that plays a fundamental role in learning, locomotion, and synaptic plasticity and is related to neurological diseases such as Parkinson's disease,

Alzheimer's disease, schizophrenia, and epilepsy.^{13,14} Thus real-time sensing of glutamate is crucial to advance basic neurological research and provides a potential pathway for diagnosing/treating neurological disorders.

Analytical techniques to determine the concentration of glutamate include capillary electrophoresis, mass spectrometry, and chromatographic and potentiometric titration.^{15–17} These techniques can be tedious, time consuming, limited in their temporal/spatial resolution, and not amenable to real-time monitoring. In contrast, electrochemical biosensors offer real-time sensing of clinically important biomolecules at low-cost and minimal power requirements, which is ideal for decentralized point-of-care facilities and implantable or hand-held devices.¹⁸

Research in the immobilization of enzymes such as GluOx provides critical knowledge for the development of biosensors, and techniques such as covalent linking,¹⁹ adsorption,^{20,21} and polymer entrapment²² are commonly used. Research over the last decade has demonstrated that incorporation of nanomaterials can significantly improve enzyme-based biosensor performance. Thus, a comprehensive understanding of the effect(s) of both enzyme immobilization and nanomaterial deposition is required to enhance the design of enzymatic biosensors.

Nanomaterials such as carbon nanotubes and metal nanoparticles can improve the sensitivity and response time of electrochemical biosensors towards the sensing of glucose,^{23,24} DNA,²⁵ and proteins.²⁶ In particular, single-walled carbon nanotubes (SWCNTs) facilitate enhanced electrochemical transduction with enzymes and demonstrate inherent electrocatalytic properties for the redox reactions of hydrogen peroxide

^aBirk Nanotechnology Center and Bindley Bioscience Center, Purdue University, West Lafayette, IN, 47907-2057, USA

^bDepartment of Agricultural and Biological Engineering, Purdue University, 225 South University Street, West Lafayette, IN, 47907-2093, USA. E-mail: porterf@purdue.edu; Fax: +(765) 494-1115; Tel: +(765) 494-1190

^cSchool of Mechanical Engineering, Purdue University, 585 Purdue Mall, West Lafayette, IN, 47907-2088, USA

^dWeldon School of Biomedical Engineering, Purdue University, 206 S. Marting Jischke Drive, West Lafayette, IN, 47907-2032, USA

(H₂O₂) and the reduced cofactor nicotinamide adenine dinucleotide (NADH), the respective enzymatic products of glutamate oxidase (GluOx) and glutamate dehydrogenase (GluDH).²⁷ Recently, electrochemical glutamate biosensors based on SWCNTs have reported some of the best glutamate sensing capabilities in terms of linear sensing range and detection limit,^{28,29} and the combination of SWCNTs with metal nanoparticles have further extended performance.³⁰

The reported SWCNT and SWCNT/metal nanoparticle glutamate biosensors previously mentioned show great promise towards sensitive glutamate sensing required for the medical and biological science fields. However, a scalable biosensor fabrication technique suitable for implantable and *in vitro* neuronal devices is still lacking. Immobilizing SWCNTs on electrodes often requires exhaustive chemical treating, washing, sorting, and filtering that increase fabrication time and cost while reducing repeatability. Moreover, SWCNTs cast or immobilized on electrode surfaces do not ensure electrical conductivity nor are they electrically connected in parallel as individual nanoelectrodes. Various chemical linking strategies are available to decorate CNTs with Pt and Pd nanoparticles.^{31,32} However, these techniques involve laborious chemical steps that are not only time consuming, they also can introduce impurities into the nanoparticles or onto the CNT sidewalls that can potentially reduce the catalytic properties of the biosensor.³³ Additionally, electrochemical CNT-based glutamate biosensors that utilize artificial electron mediators such as ferrocene can be cytotoxic thus creating complications for *in vivo* or *in vitro* neuronal glutamate sensing devices.

Herein we present two glutamate SWCNT/metal nanoparticle biosensors that are developed from the bottom-up with SWCNTs grown *in situ* from a semi-ordered template fabricated on the sensing platform itself. We create Pd nanocubes and Pt nanospheres at SWCNT defect sites through a straightforward electrodeposition process. These electrodes are subsequently transformed into glutamate biosensors *via* a GluOx drop coat biofunctionalization procedure that requires no artificial electron mediators. The rate of electron transfer, effective surface area, and biosensing performance (*i.e.*, sensitivity, detection limit, and linear sensing range) of each glutamate biosensor is monitored through cyclic voltammetric and amperometric measurements.

Experimental methods

SWCNT template fabrication

A porous anodic alumina (PAA) substrate is developed for subsequent SWCNT synthesis as outlined in our previous work.^{23,24,34–36} First, a thin film metal stack [Ti (100 nm), Al (100 nm), Fe (1 nm), and Al (400 nm)] is e-beam evaporated on an oxidized silicon wafer [P < 100 > Si (5 μm), SiO₂ (500 nm)] at a base pressure of 5.0 × 10⁻⁷ Torr. The metalized substrate is subsequently anodized by immersion in 0.3 M oxalic acid (1.5 °C) with a bias of 40 V *versus* a Pt gauze auxiliary electrode. The anodization process creates semi-ordered pores (20 nm dia.) that extend through the Al/Fe/Al layers to the Ti layer (the bottom electrical contact for the electrode) and converts the Al layers into the dielectric Al₂O₃. An electrically conductive contact pad comprised of the evaporated metals is created for

subsequent electrochemical testing by leaving a portion of the sample un-anodized.

Definition of sensor area

In order to create equally-sized (0.25 cm²) electrodes for subsequent electrochemical biosensing, the substrates are diced with a diamond-blade dicing saw (Disco DAD-2H/6). Next, the diced substrates are solvent cleaned with acetone and methanol and gently dried under a N₂ stream before SWCNT synthesis.

SWCNT synthesis

SWCNTs are grown from the Fe catalyst embedded within the pores of the PAA by microwave plasma chemical vapor deposition (MPCVD) with a SEKI AX5200S MPCVD reactor. The anodized substrate is placed in the reactor on a 5.1 cm diameter molybdenum puck and heated in a hydrogen ambient by a 3.5 kW radio-frequency power supply to 900 °C. A hydrogen plasma is generated over the sample *via* a 5 kW ASTeX AX2100 microwave generator, and methane (CH₄) gas, the acting precursor for carbon nanotube (CNT) growth, is introduced into the chamber for 10 min. The hydrogen plasma decomposes the methane gas to permit CNT growth and penetrates the oxide layer at the base of the pores of the PAA. The 10 min plasma/methane reaction creates SWCNTs, 10–50 μm in length, that extend vertically from the pores of the PAA and eventually come to rest horizontally on the PAA surface.

Pd nanocube and Pt nanosphere formation

Electrodeposition of Pd and Pt onto the electrode surface is carried out by a 3-electrode set-up (BASi Epsilon Cell Stand) where Pt gauze acts as the auxiliary electrode, Ag/AgCl as the reference electrode, and initially Ti located at the bottom of the pores as the working electrode. Pulsed electrical currents of 6 mA cm⁻² (Pd electrodeposition) and 2 mA cm⁻² (Pt electrodeposition) at 500 ms are applied between the working electrode (SWCNTs/PAA) and auxiliary electrode (Pt gauze) within baths of 2 mM PdCl₂ (Sigma Aldrich 323373) in 0.1 M HCl (J.T. Baker 9539-03) and 4 mM H₂PtCl₆·6H₂O (Sigma Aldrich 206083) in 0.5 M Na₂SO₄ (Fluka 71960) respectively. After 250 cycles of the aforementioned pulsed electrical currents the respective Pd and Pt electrodepositions partially fill the pores of the PAA, creating an electrical back contact to the SWCNTs by connecting the Ti bottom layer and Fe layer, and form distinctly shaped Pd nanocubes (150 nm width) and Pt nanospheres (150 nm dia.) at SWCNT defect sites (Fig. 1). In our experience, Pt and Pd current pulse electrodepositions consistently form nanospheres and nanocubes respectively on the individual SWCNT strands.

Glutamate oxidase (GluOx) immobilization

Glutamate oxidase (GluOx) (Seikagaku 100645-1) is first mixed with a 1% (w/v) bovine serum albumin (BSA) solution and subsequently cross-linked with glutaraldehyde by adding 0.125% (w/v) glutaraldehyde. This GluOx/BSA/glutaraldehyde solution is then drop coated onto the surface of the electrode (2 μL aliquots per electrode) and allowed to dry several hours at room temperature before electrochemical sensing.

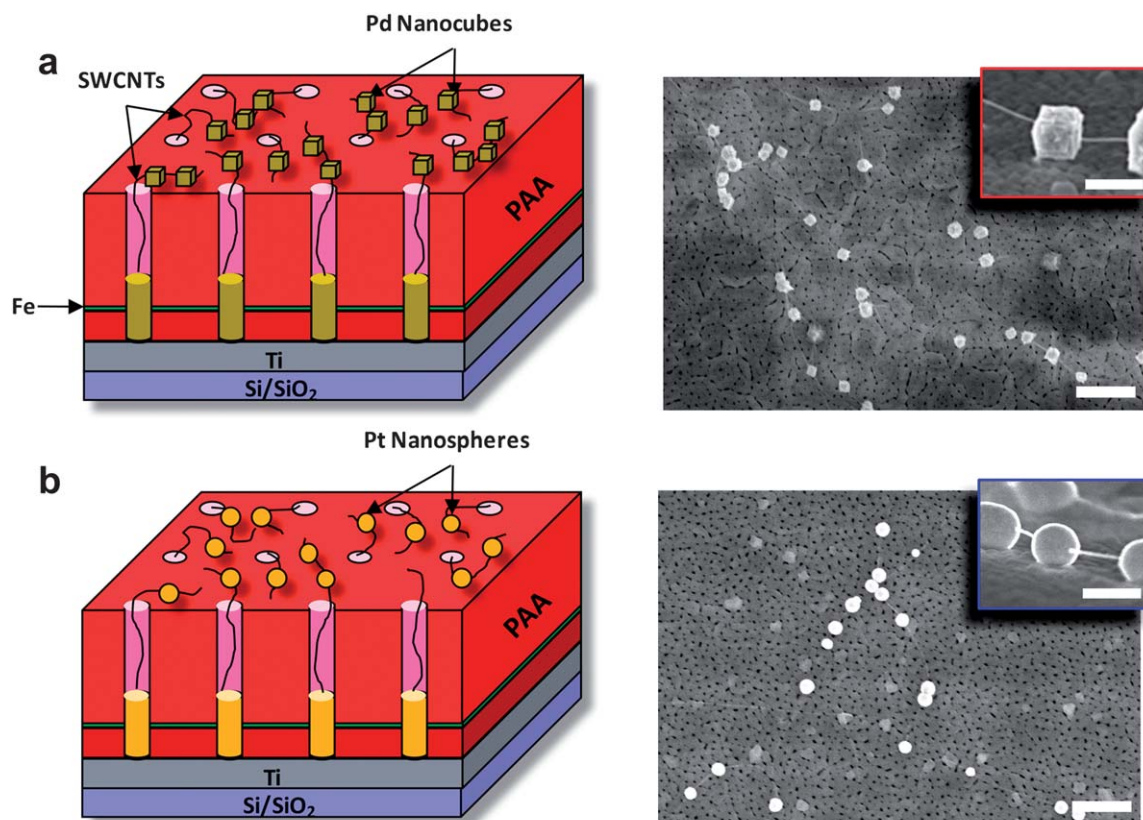


Fig. 1 Tilted cross-sectional schematics with accompanying top-view field emission electron microscopy (FESEM) micrographs and side-view high magnification micrographs as insets portraying the (a) Pd-SWCNT/PAA and (b) Pt-SWCNT/PAA electrodes. Top-view FESEM micrographs scale bars correspond to 800 nm while side-view (insets) scale bars correspond to 200 nm.

The biofunctionalized electrodes (*i.e.*, the GluOx/Pd-SWCNT/PAA and GluOx/Pt-SWCNT/PAA biosensors) are stored at 4 °C when electrochemical experimentation is not being performed.

Electrochemical measurements and set-up

A BASi Epsilon Three-Electrode Cell Stand was utilized to amperometrically sense H_2O_2 and L-glutamate. The respective GluOx/Pd-SWCNT/PAA and GluOx/Pt-SWCNT/PAA biosensors acted as the working electrodes, Ag/AgCl as the reference electrode, and a Pt wire as the auxiliary electrode. Amperometric measurements were performed in phosphate buffered saline (PBS, 0.1 M pH 7.4) at an overvoltage of 350 mV. The un-anodized portion of the biosensor (*i.e.*, the electrical contact pad) are electrically wired to the cell stand while the underlying Ti layer electrically connects the contact pad and the metal decorated SWCNTs within the pores of the PAA. The Ti bottom layer runs throughout the base of the electrode and is electrically connected to the amperometric cell—thus when the embedded Fe within the pores of the PAA is not electrically connected to the Ti layer, *via* Pd or Pt, the SWCNT network is not in electrical contact with the amperometric cell and accordingly shows a negligible response during electrochemical sensing. The amperometric glutamate detection limit of each biosensor was determined by evaluating the response current three standard deviations from the arithmetic mean of the baseline signal achieved in PBS (3σ).

Sensor imaging

All field emission scanning electron microscopy (FESEM) micrographs were obtained by an S-4800 Hitachi microscope at a power setting of 5.0 kV. Images were obtained before the immobilization of GluOx and no additional sample processing steps were taken.

Results and discussion

Biosensor design

In an effort to increase the electroactive surface area and electrocatalytic nature of the SWCNT-based biosensors, Pd nanocubes and Pt nanospheres (150 nm in width and diameter respectively) were electrodeposited on the SWCNT networks. The average spacing of the nanocubes and nanospheres on each SWCNT strand matches the spacing of SWCNT defect sites previously reported³⁷ at 366 nm with a high standard deviation ($\sigma = 362$ nm) and overall spacing range between 50 nm and 1.2 μm (Fig. 2a and 2b). The average spacing between each metal decorated SWCNT strand is 8.0 μm ($\sigma = 6.1\mu\text{m}$) with the inter-SWCNT spacing falling within an overall range of 1 μm to 30 μm (Fig. 2c).

Cyclic voltammetry characterization

The Pt-SWCNT/PAA and Pd-SWCNT/PAA electrodes are characterized *via* cyclic voltammetry in 4 mM $\text{Fe}(\text{CN})_6^{3-}$ and

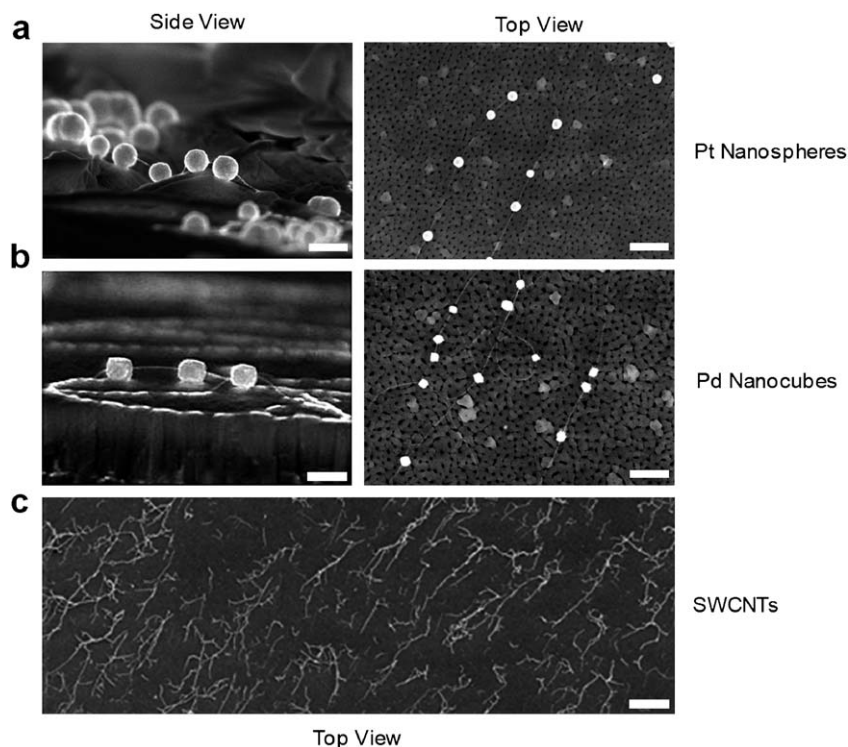


Fig. 2 Top-view and side-view FESEM micrographs of (a) Pt nanospheres and (b) Pd nanocubes electrodeposited on SWCNT arrays (white lines) on PAA illustrates the typical distance between metallic nanoparticles on individual SWCNT strands. (c) The distance between SWCNTs strands is portrayed in the top-view FESEM micrograph of SWCNTs resting on PAA (note: SWCNTs were coated with electrodeposited Pd in order to visually observe the SWCNTs with FESEM). Side-view and top-view Pt nanosphere and Pd nanocube FESEM micrograph scale bars (a–b) correspond to 250 nm and 800 nm respectively while the top-view SWCNTs FESEM micrograph scale bar (c) corresponds to 20 μm .

1 M KNO_3 at a potential scan that is cycled between -0.2 V and $+0.6$ V versus a Ag/AgCl reference electrode at a 10 mV s^{-1} scan rate (Fig. 3). The cyclic voltammograms of both the Pt-SWCNT/PAA and Pd-SWCNT/PAA electrode show defined oxidation and reduction peaks with cyclic voltammetric peak-to-peak separation (ΔE_p) of 0.90 mV and 0.92 mV respectively. These

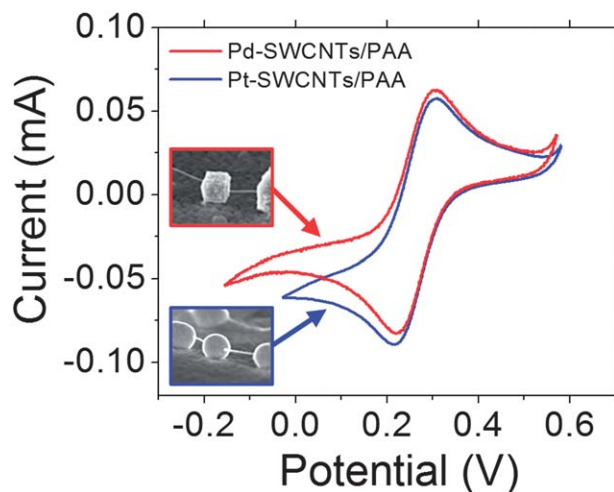


Fig. 3 Cyclic voltammograms of the (a) Pd-SWCNT/PAA and (b) Pt-SWCNT/PAA electrodes in 4 mM $\text{Fe}(\text{CN})_6^{3-}$ and 1 M KNO_3 at a potential scan that is cycled between -0.2 V and 0.6 V versus a Ag/AgCl reference electrode at a scan rate of 10 mV/s .

ΔE_p values for ferricyanide electrochemistry demonstrate much faster electron transfer rates when compared to the basal planes of highly oriented pyrolytic graphite ($\Delta E_p = 630$ mV)³⁸ and compare favorably with similar CNT-based electrodes where aligned MWCNTs and horizontally oriented SWCNT paper electrodes have reported ΔE_p values of 230 mV and 96 mV respectively.³⁹

The electroactive surface area of the Pt-SWCNT/PAA and Pd-SWCNT/PAA biosensors can be calculated by using the Randles-Sevcik equation.⁴⁰

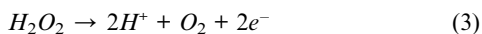
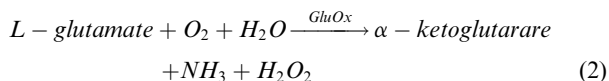
$$i_p = 2.69 \times 10^5 A D^{\frac{1}{2}} n^{\frac{3}{2}} \nu^{\frac{1}{2}} C \quad (1)$$

where n is the number of participating electrons in the redox reaction ($n = 1$), A is the effective electroactive electrode surface area (cm^2), D is the diffusion coefficient of the molecule in solution (6.70×10^{-6} $\text{cm}^2 \text{s}^{-1}$), C is the concentration of the target molecule in the bulk solution (4 mM), ν is the scan rate (V s^{-1}), and i_p is the current (A) at the reduction peak. The calculated effective electroactive surface area for the Pt-SWCNT/PAA and Pd-SWCNT/PAA electrodes is nearly identical, $(2.06 \pm 0.5) \times 10^{-4}$ cm^2 and $(2.25 \pm 0.5) \times 10^{-4}$ cm^2 respectively, allowing for a more accurate comparison during subsequent electrochemical sensing.

Amperometric measurement of hydrogen peroxide (H_2O_2)

Electrochemical glutamate biosensors biofunctionalized with the enzyme GluOx typically measure L-glutamate concentrations via

the electrochemical detection of H_2O_2 produced during the GluOx/glutamate reaction. The chemical reactions associated with the enzymatic breakdown of glutamate and the subsequent oxidation of the H_2O_2 produced from this reaction are as follows:



In order to demonstrate the effectiveness of the Pt-SWCNT/PAA and Pd-SWCNT/PAA electrodes towards electrochemical glutamate biosensing, both sensors are first biofunctionalized with GluOx cross-linked with glutaraldehyde and bovine serum albumin (BSA) and subsequently utilized in amperometric H_2O_2 sensing (Fig. 4). All electrochemical measurements are performed in 20 mL of phosphate buffered saline (PBS, pH = 7.4) via a 3 electrode set-up (BASi Epsilon Cell Stand). Successive 20 μL aliquots of H_2O_2 are added to the PBS to increase the H_2O_2 concentration by 10 μM increments while the redox current associated with the oxidation of H_2O_2 is measured at a working potential of 350 mV. The GluOx/Pt-SWCNT/PAA biosensor exhibited a sensitivity of $72.4 \mu\text{A mM}^{-1} \text{cm}^{-2}$ towards the oxidation of H_2O_2 , which is over four times the sensitivity of the GluOx/Pd-SWCNT/PAA biosensor ($16.8 \mu\text{A mM}^{-1} \text{cm}^{-2}$). The GluOx/SWCNT/PAA biosensor displayed a negligible response towards H_2O_2 because the SWCNTs are not electrically contacted to the Ti bottom layer by Pd or Pt (see **Experimental Section**).

Amperometric measurement of glutamate

Amperometric glutamate sensing for both the GluOx/Pd-SWCNT/PAA and GluOx/Pt-SWCNT/PAA biosensors is conducted under the same 3-electrode set-up and working potential (350 mV) established during the amperometric H_2O_2 testing. Amperometric glutamate calibration plots are created by adding successive aliquots of increasing glutamate concentrations and measuring the corresponding steady-state signal current response, typically achieved within 5 s, of the biosensor (Fig. 5). The amperometric glutamate calibration plots (Fig. 5a and 5d) and experimental detection limit plots (Fig. 5c and 5f) are illustrated. As a control experiment, PBS (0.1M, pH 7.4) is injected at equivalent volumes to glutamate injections to demonstrate current response originates from glutamate and not the buffered media itself even at the lowest detectable glutamate concentration steps (Fig. 5c and 5f).

The GluOx/Pt-SWCNT/PAA biosensor exhibited a wide linear sensing region extending from 50 nM to 1.6 mM with a detection limit of 4.6 nM (3σ) while the GluOx/Pd-SWCNT/PAA biosensor portrayed a linear sensing region from 1 to 250 μM with a detection limit of 180 nM (3σ). Furthermore the GluOx/Pt-SWCNT/PAA biosensor demonstrates a glutamate sensitivity ($27.4 \mu\text{A mM}^{-1} \text{cm}^{-2}$) that is nearly five times the sensitivity of the GluOx/Pd-SWCNT/PAA biosensor ($5.5 \mu\text{A mM}^{-1} \text{cm}^{-2}$). These experimental results demonstrate the effectiveness of these SWCNT/metal nanoparticles biosensors in amperometric glutamate biosensing and their sensing capabilities

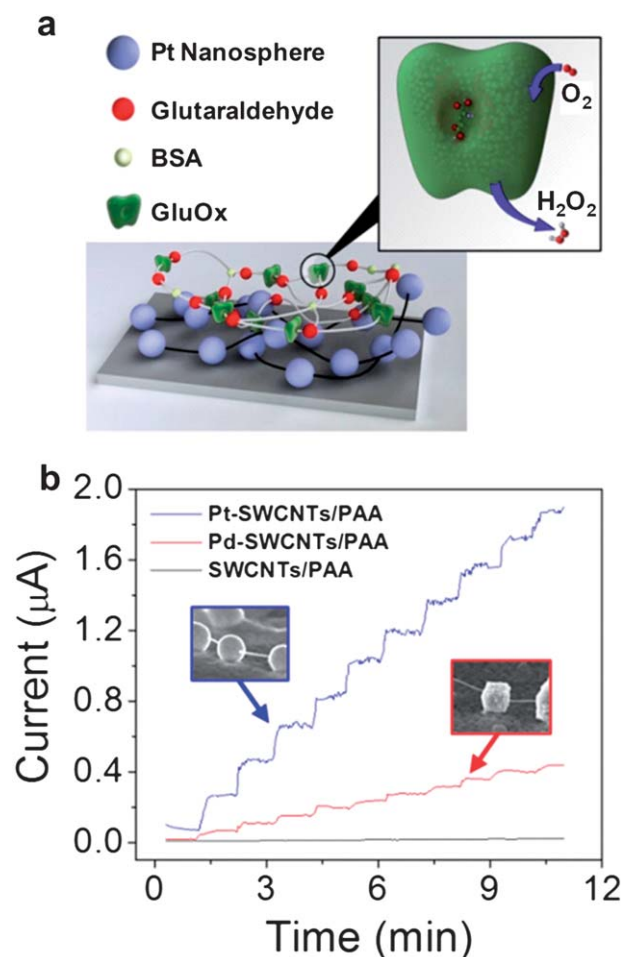


Fig. 4 Electrode biofunctionalization scheme and H_2O_2 calibration plots. (a) A side-view schematic diagram illustrating GluOx cross-linked with glutaraldehyde and BSA immobilized on networks of Pt nanospheres connected by SWCNTs (**black lines**). Inset: Magnified view of a single GluOx enzyme. Glutamate binds within the enzymatic pocket of GluOx while O_2 is consumed, producing the electrochemical transducer H_2O_2 . (b) Amperometric sensing of H_2O_2 oxidation in 20 mL of PBS (pH 7.4) using a three electrode potentiostat with an applied working potential of 350 mV. The current response for incremental H_2O_2 concentration increases of 10 μM are recorded for the GluOx/Pt-SWCNT/PAA (**blue**), GluOx/Pd-SWCNT/PAA (**red**), and GluOx/SWCNTs/PAA (**black**) biosensors.

proved exemplary when compared to similar electrochemical glutamate biosensors including those based on CNTs, metal nanoparticles, and conventional electrode materials such as glassy carbon (Table 1.).

Conclusions

In this work, we performed a side-by-side comparison between SWCNT-based glutamate biosensors augmented with Pd nanocubes and Pt nanospheres. By utilizing a bottom-up *in situ* approach to biosensor fabrication, we were able to grow low-density arrays of SWCNTs directly on the biosensor surface and electrodeposit Pd nanocubes and Pt nanospheres along the

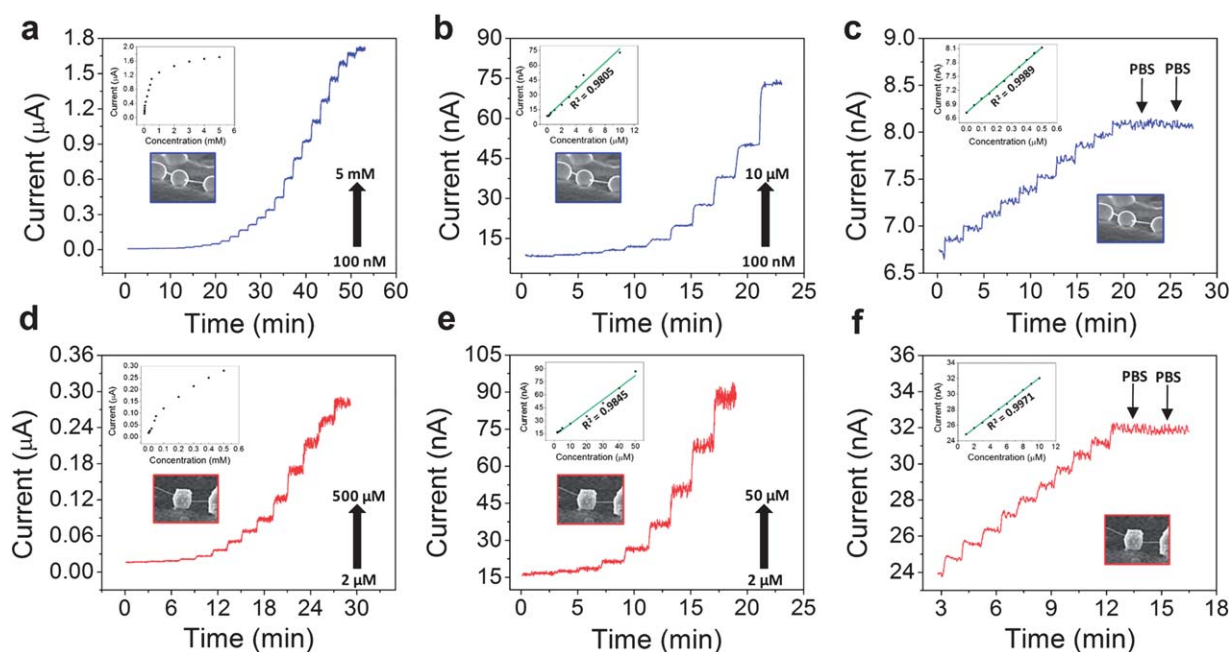


Fig. 5 Amperometric glutamate calibration plots for the GluOx/Pt-SWCNT/PAA (a–c) and GluOx/Pd-SWCNT/PAA (d–f) biosensors with insets that portray current vs. concentration profiles. (a) Current response for successive glutamate concentration increases of 100–500 nM by 100 nM, 1–5 μ M by 1 μ M, 10–50 μ M by 10 μ M, 100–500 μ M by 100 μ M, and finally 1–5 mM by 1 mM. (d) Current response for successive glutamate concentration increases of 2–5 μ M by 1 μ M, 10–50 μ M by 10 μ M, and 100–500 μ M by 100 μ M. Corresponding magnified views, (b) and (e) represent the lower end of the respective calibration plots portraying a portion of the linear sensing region with insets showing linear regression analysis of the current vs. concentration profiles. Current response for 10 successive 20 μ L glutamate injections resulting in incremental concentration increases of (c) 50 nM and (f) 1 μ M followed by two 20 μ L injections of PBS (0.1M, pH 7.4), while insets show linear regression analysis of the current vs. concentration profiles.

individual SWCNTs with an average spacing of 366 nm ($\sigma = 362$ nm). In order to make a more accurate comparison between the two distinct biosensors, we equalized the effective surface area and immobilized enzyme by creating similarly sized Pd nanocubes (width = 150 nm) and Pt nanospheres (diameter = 150 nm) through a controlled electrodeposition process and by subsequently drop coating equal aliquots of GluOx enzyme cross-linked with glutaraldehyde on each biosensor surface. The Pt nanosphere/SWCNT glutamate biosensor outperformed the Pd nanocube/SWCNT biosensor and similar CNT, metal

nanoparticle/CNT, and conventional material based glutamate biosensors in terms of linear sensing range and detection limit.

We believe these results are due to the unique hybrid nature (*i.e.*, CNTs combined with metallic nanoparticles) of the biosensor and to the shape and composition of the metal constituents. The SWCNTs rest above the surface of the PAA and subsequently permit metallic nanoparticles to grow concentrically around the SWCNTs defect sites^{23,24,37}—allowing for the formation of uniquely shaped nanostructures (*e.g.*, spheres and cubes) above the surface of the PAA. Thus the

Table 1 Electrochemical performance comparison of CNT, metal nanoparticle/CNT, and conventional material based glutamate biosensors^{a,b,c}

Biosensor Description	Detection Limit (nM)	Linear Range (μ M)	Ref.
GluOx/Pt-SWCNT/PAA	4.6	0.05–1600	*
GluOx/Pd-SWCNT/PAA	180	1–250	*
Ferrocene-SWCNT/Pt	—	1–7	28
GluDH-Thionine-SWCNT/GC	100	0.5–400	29
(GluDH/Pt-PAMAM) _n /CNTs/GC	10	0.2–250	30
GluOx-poly- <i>m</i> -PD/MWCNT/W	—	100–500	41
GluOx-Nafion/GC	100	0.1–100	42
GluOx-Chitosan/Pt	100	0.5–200	43
GluOx-HRP-PEGDGE/Au	500	up to 60	44
GluOx-Nafion-MV/GC	20,000	up to 750	45

^a A dash (-) in a column represents a value that is not reported in the respective reference. ^b An asterisk (*) in a column refers to the work presented in this manuscript. ^c Abbreviations: (GluOx) glutamate oxidase, (Pt) platinum, (Pd) pladium, (SWCNT) single-walled carbon nanotube, (PAA) porous anodic alumina, (GluDH) glutamate dehydrogenase, (Pt-PAMAM) Poly(amidoamine dendrimer-encapsulated platinum nanoparticles, (GC) glassy carbon, (*m*-PD) *m*-phenylenediamine, (W) tungsten, (HRP) horseradish peroxidase, (PEGDGE) Poly(ethylene glycol)(400)diglycidyl ether, (Au) gold, (MV) methyl viologen.

metallic nanoparticles are fully exposed to incoming species during electrochemical sensing and are electrically connected *via* highly conductive SWCNTs. Therefore these metallic nanoparticle/SWCNT networks create large arrays of electro-reactive nanoelectrodes which typically experience larger current densities, improved signal-to-noise ratios, and higher sensitivities than micro/macro electrodes.^{46,47}

The unique shape and material composition of the Pt nanospheres and Pd nanocubes may help to explain the performance disparity between the Pt nanosphere/SWCNT and Pd nanocube/SWCNT glutamate biosensors. For example, recent studies have shown that “near spherical” Pt nanoparticles, similar in shape to the Pt nanospheres presented herein (Fig. 2a), are composed of numerous facets with more surface atoms located at the interfaces of these facets than those with cubic shape.⁴⁸ Accordingly, these “near spherical” nanoparticles exhibit higher catalytic activity than their cubical counterparts.⁴⁹ Furthermore, enzymatic glucose and glutamate biosensors have demonstrated higher sensitivities with Pt-based electrodes than Pd-based.^{50,51} These recent reports corroborate the sensing results presented herein, where the Pt nanosphere/SWCNT biosensor displayed a higher sensitivity to the oxidation of H₂O₂ and subsequently a higher glutamate sensitivity than the Pd nanocube/SWCNT biosensor. Thus both the shape and material composition of the Pt nanospheres may have contributed to the enhanced performance of the Pt nanosphere/SWCNT glutamate biosensor.

The hybrid metal nanoparticle/SWCNT glutamate biosensors are potentially well-suited for neurological research. Both developed metal nanoparticle/SWCNT glutamate biosensors demonstrate the potential capability to measure extracellular glutamate concentrations (1–2 μM) that have previously been measured within brain tissue using microscale techniques.⁵² However, these microscale techniques grossly overestimate glutamate concentrations found in the tripartite synaptic environment (*i.e.* space formed by pre- and post-synaptic neurons and neighboring astrocytes/oligodendrocytes).⁵³ The unique nanoenvironment interface of our metal nanoparticle/SWCNT biosensors (SWCNTs 1–3 nm in diameter and nanospheres and nanocubes 150 nm in diameter and width respectively) are on the same order of magnitude of the synaptic cleft region (20–50 nm), and thus offer a nanoscale interface that could improve the accuracy of glutamate sensing within the tripartite synaptic environment over current microscale monitoring techniques. Furthermore, SWCNTs incorporated into neurological devices can stimulate the growth of neurons and modulate their behavior—presenting an amenable interface with neurons.⁵⁴ Thus the concomitance of the low detection limit (4.6 nM), wide linear sensing range (50 nM to 1.6 mM), and unique nanoenvironment of the Pt nanosphere/SWCNT hybrid biosensor could act synergistically to more accurately monitor neurotransmitter release/uptake.

In future work we will operate and test the sensor in human serum solutions. Selectivity experiments will monitor the effects of endogenous electroactive species (*e.g.*, ascorbic acid, uric acid, acetaminophen) that may cause potential electrochemical interference during sensor operation. Anion repellants (*e.g.*, Nafion) may be added to the sensor fabrication protocol in order to block or minimize said interference. Future work will also entail biosensor life-time sensing where the sensor sensitivity will be

monitored for several weeks within *in vitro* and/or *in vivo* environments in order to test the stability and activity of the enzymes over extended periods of time.

Acknowledgements

The authors would like to gratefully acknowledge assistance from the Purdue Nanoscale Transport Research Group of the Birck Nanotechnology Center and the Purdue Physiological Sensing Facility of the Bindley Bioscience Center. We graciously recognize funding support from the Office of Naval Research, National Science Foundation, and the Purdue Research Foundation Trask Fund. A special thanks is also extended to Michel Schweinsberg for assistance in schematic diagram illustrations.

References

- 1 P. Alivisatos, *Nat. Biotechnol.*, 2004, **22**, 47–52.
- 2 K. Balasubramanian and M. Burghard, *J. Mater. Chem.*, 2008, **18**, 3071–3083.
- 3 R. J. Chen, S. Bangsaruntip, K. A. Drouvalakis, N. Wong Shi Kam, M. Shim, Y. Li, W. Kim, P. J. Utz and H. Dai, *Proc. Natl. Acad. Sci. U. S. A.*, 2003, **100**, 4984–4989.
- 4 Y. Lin, F. Lu, Y. Tu and Z. Ren, *Nano Lett.*, 2004, **4**, 191–195.
- 5 H. Lord and S. O. Kelley, *J. Mater. Chem.*, 2009, **19**, 3127–3134.
- 6 J. Wang, *Analyst*, 2005, **130**, 421–426.
- 7 W. U. Wang, C. Chen, K. Lin, Y. Fang and C. M. Lieber, *Proc. Natl. Acad. Sci. U. S. A.*, 2005, **102**, 3208.
- 8 K. T. Yong, I. Roy, M. T. Swihart and P. N. Prasad, *J. Mater. Chem.*, 2009, **19**, 4655.
- 9 C. Da, G. Wang and J. Li, *J. Phys. Chem. C*, 2007, **111**, 2351–2367.
- 10 I. M. Feigel, H. Vedala and A. Star, *J. Mater. Chem.*, 2011, **21**, 8940–8954.
- 11 L. Soleymani, Z. Fang, E. H. Sargent and S. O. Kelley, *Nat. Nanotechnol.*, 2009, **4**, 844–848.
- 12 T. M. Squires, R. J. Messinger and S. R. Manalis, *Nat. Biotechnol.*, 2008, **26**, 417.
- 13 C. Holden, *Science*, 2003, **300**, 1866–1868.
- 14 M. Nedergaard, T. Takano and A. J. Hansen, *Nat. Rev. Neurosci.*, 2002, **3**, 748–755.
- 15 L. A. Dawson, J. M. Stow and A. M. Palmer, *J. Chromatogr., Biomed. Appl.*, 1997, **694**, 455–460.
- 16 T. Gunduz, N. Gunduz, E. Kilic, F. Koseoglu and S. Guloztas, *Analyst*, 1988, **113**, 715.
- 17 R. S. Walikonis, O. N. Jensen, M. Mann, D. W. Provance Jr, J. A. Mercer and M. B. Kennedy, *J. Neurosci.*, 2000, **20**, 4069.
- 18 J. Wang, *Biosens. Bioelectron.*, 2006, **21**, 1887–1892.
- 19 T. Wink, S. J. Van Zuilen, A. Bult and W. P. Van Bennekom, *Analyst*, 1997, **122**, 43R–50R.
- 20 M. Ferreira, P. A. Fiorito and O. N. Oliveira, *Biosens. Bioelectron.*, 2004, **19**, 1611–1615.
- 21 S. S. Kim, P. B. Amama and T. S. Fisher, *J. Phys. Chem. C*, 2010, **114**, 9596–9602.
- 22 S. Cosnier, *Anal. Bioanal. Chem.*, 2003, **377**, 507–520.
- 23 J. C. Claussen, A. D. Franklin, A. ul Haque, D. M. Porterfield and T. S. Fisher, *ACS Nano*, 2009, **3**, 37–44.
- 24 J. C. Claussen, K. S. Sungwon, A. u. Haque, M. S. Artilles, D. M. Porterfield and T. S. Fisher, *J. of Diabetes Sci. and Technol.*, 2010, **4**, 312–319.
- 25 J. Wang, G. Liu and M. R. Jan, *J. Am. Chem. Soc.*, 2004, **126**, 3010–3011.
- 26 J. J. Gooding, R. Wibowo, J. Liu, W. Yang, D. Losic, S. Orbons, F. J. Mearns, J. G. Shapter and D. B. Hibbert, *J. Am. Chem. Soc.*, 2003, **125**, 9006–9007.
- 27 E. E. Katz and I. I. Willner, *ChemPhysChem*, 2004, **5**, 1084–1104.
- 28 X. J. Huang, H. S. Im, D. H. Lee, H. S. Kim and Y. K. Choi, *J. Phys. Chem. C*, 2007, **111**, 1200–1206.
- 29 L. Meng, P. Wu, G. Chen, C. Cai, Y. Sun and Z. Yuan, *Biosens. Bioelectron.*, 2009, **24**, 1751–1756.

- 30 L. Tang, Y. Zhu, L. Xu, X. Yang and C. Li, *Talanta*, 2007, **73**, 438–443.
- 31 Z. Liu, X. Lin, J. Y. Lee, W. Zhang, M. Han and L. M. Gan, *Langmuir*, 2002, **18**, 4054–4060.
- 32 V. Lordi, N. Yao and J. Wei, *Chem. Mater.*, 2001, **13**, 733–737.
- 33 D.-J. Guo and H.-L. Li, *J. Electroanal. Chem.*, 2004, **573**, 197–202.
- 34 J. C. Claussen, M. M. Wickner, T. S. Fisher and D. M. Porterfield, *ACS Appl. Mater. Interfaces*, 2011, **3**, 1765–1770.
- 35 A. D. Franklin, D. B. Janes, J. C. Claussen, T. S. Fisher and T. D. Sands, *Appl. Phys. Lett.*, 2008, **92**, 013122.
- 36 M. R. Maschmann, A. D. Franklin, A. Scott, D. B. Janes, T. D. Sands and T. S. Fisher, *Nano Lett.*, 2006, **6**, 2712–2717.
- 37 Y. Fan, B. R. Goldsmith and P. G. Collins, *Nat. Mater.*, 2005, **4**, 906–911.
- 38 R. R. Moore, C. E. Banks and G. Richard, *Anal. Chem.*, 2004, **76**, 2677–2682.
- 39 J. Li, A. Cassell, L. Delzeit, J. Han and M. Meyyappan, *J. Phys. Chem. B*, 2002, **106**, 9299–9305.
- 40 A. J. Bard and L. R. Faulkner, *Electrochemical Methods. Fundamentals and Applications*, John Wiley, New York, 2001.
- 41 H. Boo, R. A. Jeong, S. Park, K. S. Kim, K. H. An, Y. H. Lee, J. H. Han, H. C. Kim and T. D. Chung, *Anal. Chem.*, 2006, **78**, 617–620.
- 42 A. A. Karyakin, E. E. Karyakina and L. Gorton, *Anal. Chem.*, 2000, **72**, 1720–1723.
- 43 M. Zhang, C. Mullens and W. Gorski, *Electrochim. Acta*, 2006, **51**, 4528–4532.
- 44 J. Castillo, A. Blöchl, S. Dennison, W. Schuhmann and E. Csöregi, *Biosens. Bioelectron.*, 2005, **20**, 2116–2119.
- 45 R. Maalouf, H. Chebib, Y. Saïkali, O. Vittori, M. Sigaud and N. Jaffrezic-Renault, *Biosens. Bioelectron.*, 2007, **22**, 2682–2688.
- 46 D. W. M. Arrigan, *Analyst*, 2004, **129**, 1157–1165.
- 47 R. G. Compton, G. G. Wildgoose, N. V. Rees, I. Streeter and R. Baron, *Chem. Phys. Lett.*, 2008, **459**, 1–17.
- 48 R. Narayanan and M. A. El-Sayed, *J. Phys. Chem. B*, 2005, **109**, 12663–12676.
- 49 R. Narayanan and M. A. El-Sayed, *Nano Lett.*, 2004, **4**, 1343–1348.
- 50 J. Lu, I. Do, L. T. Drzal, R. M. Worden and I. Lee, *ACS Nano*, 2008, **2**, 1825–1832.
- 51 R. D. O’Neill, S. C. Chang, J. P. Lowry and C. J. McNeil, *Biosens. Bioelectron.*, 2004, **19**, 1521–1528.
- 52 B. K. Day, F. Pomerleau, J. J. Burmeister, P. Huettl and G. A. Gerhardt, *J. Neurochem.*, 2006, **96**, 1626–1635.
- 53 B. Zuber, I. Nikonenko, P. Klauser, D. Muller and J. Dubochet, *Proc. Natl. Acad. Sci. U. S. A.*, 2005, **102**, 19192.
- 54 E. B. Malarkey, K. A. Fisher, E. Bekyarova, W. Liu, R. C. Haddon and V. Parpura, *Nano Lett.*, 2009, **9**, 264–268.